

MASS IDENTIFICATION IN HEAVY ION COLLECTION WITH THE
SPECTROMETER SOLENO

E. HOURANI, J. KUMPULAINEN*, F. AZAEIZ**, S. FORTIER,
S. GALES, J.M. MAISON, P. MASSOLO***, B. RAMSTEIN AND
J.P. SCHAPIRA

I.P.N. BP n°1, 91406 Orsay Cedex, FRANCE

* University of Jyväskylä, Jyväskylä, FINLAND

** CEN de Bordeaux-Gradignan, 33170 Gradignan, FRANCE

***Member of the Conicet, on leave from the university
of La Plata, ARGENTINA

IPNO-DRE 87-27

MASS IDENTIFICATION IN HEAVY ION COLLECTION WITH
THE SPECTROMETER SOLENO

E. HOURANI, J. KUMPULAINEN*, F. AZAIEZ**, S. FORTIER, S. GALES,
J.M. MAISON, P. MASSOLO***, B. RAMSTEIN AND J.P. SCHAPIRA.

Institut de Physique Nucléaire BP n° 1, 91406 Orsay Cedex, FRANCE

ABSTRACT

A detection system consisting of a thin film scintillator detector and a solid state detector has been set up and used to measure the time of flight and energy of the fusion evaporation residues collected with the magnetic spectrometer SOLENO at the Orsay Tandem. The linear responses and the timing properties of the system were tested using a ^{252}Cf source and beams of ^{16}O , ^{32}S and ^{58}Ni . The system was used to study the mass identification and the collection yield obtained with SOLENO.

* Present adress : University of Jyvaskyla, Jyvaskyla, Finland.

** Present adress : Centre d'Etudes de Bordeaux-Gradignan, Le Haut-Vigneau, 33170 Gradignan, France.

*** Member of the Conicet, on leave from the University of La Plata, Argentina.

1. INTRODUCTION

The superconducting solenoidal coil SOLENO¹⁾ operating near zero degrees with respect to the beam of the MP Tandem at Orsay was studied as a recoil mass spectrometer. Fusion evaporation residues of masses up to $A \sim 70$ were collected by the spectrometer and implanted into a detector located in its image plane. The subsequent fast decay (100 ns - 50 ms) of the implanted residues by emission of light charged particles (p and α) is under investigation. In order to study the properties of the spectrometer in heavy ion collection, we used a detection system providing an identification in mass for the collected ions. This system consists of a Thin Film scintillator Detector (TFD) placed at the entrance of the spectrometer and a Solid State Detector (SSD) located in the image plane (Fig.1). The film gives a time measurement and the SSD gives time and energy measurements, thus achieving the time of flight and energy measurements necessary in mass identification.

A TFD was chosen as a zero-time detector placed at the entrance of the spectrometer because it is probably the unique common detector which could fulfil simultaneously the following stringent requirements :

- An active area for the detection of at least 5 cm^2 in order to match the large angular acceptance (100 msr) of the spectrometer.
- A hole at its centre for the passage of the beam towards the Faraday cup (Fig. 1).
- A fast detection response compatible with a very high counting rate due to the strong emission around zero degrees of the elastically scattered beam.

Recently, several studies of the TFD properties were reported²⁻⁸⁾ and some TFD-SSD assemblies were described⁹⁻¹⁰⁾. But systematic presentations of tests together with effective uses in heavy ion detection are scarce. The TFD remains a special product manufactured by the user with no simple standard characteristics and method of test. These facts lead us to give in the present paper a detailed description of our TFD and TFD-SSD assembly. Moreover, we would like to point out some aspects in which, we believe, we brought a significant gain towards the standardization of the TFD tests.

The basic properties of SOLENO with a preliminary test in heavy ion detection were reported ^{1,11,12}). In the present paper, the general characteristics of SOLENO in heavy ion collection have been more precisely studied along a wider range of masses and energies available in fusion evaporation residues at Tandem energies.

2. TEST OF THE TFD-SSD ASSEMBLY

The test of the TFD and SSD properties was performed without running the spectrometer SOLENO. Standard radioactive sources, i.e. ²⁴¹Am and ²⁵²Cf, together with O, S and Ni beams delivered by the Tandem were used. Special care was taken in studying the timing characteristics of the TFD which, in fact, limit the time resolution of the assembly and also in investigating the pulse height response of the TFD which mostly governs their use in heavy ion detection.

2.1 DESCRIPTION OF THE DETECTION SYSTEM

The detection system consists of the TFD and the SSD and of the associated electronic setup.

The main part of the TFD is the thin scintillator film. Our films were made by dissolving chips of SOCHIBO KL 236 scintillator in ethyl acetate. A glass plate immersed into the solution and dried was then coated on both sides with scintillator films. These films were peeled off by immersing slowly the plate in deionized water and were then lifted from the water on their final frames. The thickness of the film was measured by the energy loss of α particles emitted by an ²⁴¹Am source as well as by its weight to area ratio. Two typical thicknesses of 160 $\mu\text{g}/\text{cm}^2$ and 90 $\mu\text{g}/\text{cm}^2$ were obtained, depending on the concentration of the scintillator in the solution. The frame of the film consisted of a mirror polished aluminium plate with a circular opening where is maintained a copper wire ring (Fig. 2). The film was cut inside the ring for the passage of the beam. The light reflector consisted of a hollow aluminium cylinder with two opposite lateral openings matching, in diameters, the angular acceptance (10°) of SOLENO when the film was located at 7.5 cm from the target (Fig. 2). The

entire inner surface of the reflector was mirror polished. The film frame was placed inside the reflector along its axis and facing the two openings. The reflector was fixed on a light guide made of optical plexiglass which was optically connected to a photomultiplier of the type RTC XP 2020, as shown in figure 2.

The SSD used in this work was a surface barrier Si detector of the type ORTEC TD, 100 μm thick with an area of 300 mm^2 . Its energy resolution measured with α -particles of 5.48 MeV was 40 keV.

A diagram of the electronic setup is shown in figure 3. In general, three correlated analog signals were recorded for a particle passed through the TFD and stopped in the SSD : the TFD light output L, the energy E lost in the SSD and the time-of-flight T.

2.2 RESPONSE OF THE TFD TO RADIOACTIVE SOURCES

The single response of the TFD to the α -particles of the ^{241}Am and to the fission fragments of the ^{252}Cf source were obtained for films of the same thickness in two different configurations. In one configuration, the source placed in front of the film was collimated by a diaphragm in order to irradiate the central part of the film (which was not cut in this case). It is the response of the central part of the film which was used in this work for the comparative study of the response of the film to fission fragments and to ^{16}O , ^{32}S and ^{56}Ni particles. In the second configuration the diaphragm was taken away in order to irradiate the whole surface of the film which was cut in its central part as when used with the spectrometer SOLENO.

The responses of the central part of the film to ^{241}Am and ^{252}Cf sources are displayed in figures 4.a and 4.b respectively. With ^{241}Am source we obtain the typical response to α -particles which is so poor that there is no characteristic peak. With ^{252}Cf source, we see a resolved peak corresponding to the light fission fragments of the ^{252}Cf , the response to the heavy fragments being lower and covered by the tail due to the α -particles emitted with a high rate by the ^{252}Cf source. In figure 4.c is presented the response of the annular film to Cf source. There is still a characteristic peak but with a larger width than in the precedent case due to a stronger dispersion of the light reflected towards the photomultiplier.

2.3 RESPONSE OF THE SSD TO ^{252}Cf FISSION FRAGMENTS

We applied the method of Schmitt et al.¹³⁻¹⁴⁾ used to evaluate the SSD in heavy ion detection. Following this method, the values of some parameters describing the response of the SSD to Cf fission fragments are indicative of the detector performances. In figure 5, we present the energy spectrum given by our SSD together with the definition of some characteristic quantities, and in table 1 we report the deduced values of the descriptive parameters.

In fact, this energy spectrum was obtained for slowed fission fragments because the film of $160 \mu\text{g}/\text{cm}^2$ was kept interposed between the Cf source and the SSD in order to protect the SSD from contamination. So, for comparison, we reported in table 1 the values of the parameters expected from good detectors with unslowed fission fragments¹⁴⁾ together with values deduced from ref.7 with fission fragments slowed as much as in our case. The comparison shows that our values are quite good and do not justify suspecting neither a poor resolution nor an energy tailing for our SSD in heavy ion detection.

2.4 RESPONSE OF THE COINCIDENT TFD-SSD ASSEMBLY TO ^{252}Cf SOURCE

The TFD being placed between the Cf source and the SSD, correlated responses of the TFD and the SSD were obtained using the electronic system given in figure 3. The three parameters L, E and T indicated in the figure were recorded in event-by-event mode for each fission fragment detected in coincidence by the two detectors.

The contour plots of the correlated TFD and SSD responses are presented in figure 6. Figure 6.a displays the correlated linear responses, the energy E and the light output L. In particular, it shows the dependence of the light emission of the film on the fission fragment energy (or mass). The tendency is : lighter masses produce higher intensity of light. In figure 6.b the contour plot of the correlated L, T is given. The spread seen along the T axis is due both to the finite time resolution and to the dependence of the time-of-flight on the fragment energy. This dependence was removed by setting windows in the energy spectrum (Fig. 7.a). The corresponding contour plot is shown in figure 6.c, which gives

for the two central masses in fission fragment mass distribution the time and the light output resolutions of the coincident TFD-SSD assembly. In fact, the quantitative study of these resolutions can be better carried out in the L and T spectra (figure 7.b,c) obtained by projecting figure 6.c on the L and T axes.

To see how much the dependence of the T on E was removed by setting the E windows, let us use an expression that we deduced from the results of ref.13 on Cf fission fragments and which relates different quantities defined in figure 7 :

$$\frac{\Delta T_L}{T_H - T_L} = 0.65 \frac{\Delta E_L}{E_L - E_H} \quad \text{and} \quad \frac{\Delta T_H}{T_H - T_L} = 1.02 \frac{\Delta E_H}{E_L - E_H} \quad (1)$$

Taking into account the widths of the E windows set such that $\Delta E_L / (E_L - E_H) = \Delta E_H / (E_L - E_H) = 1/10$ and the distance of about 3 cm between the TFD and the SSD giving a value of $T_H - T_L$ of about 0.91 ns, we conclude that there is no important contribution ($\lesssim 0.1$ ns) originating from the width of the E window.

On the other hand we considered our SSD as being good enough to give a negligible intrinsic contribution in the T resolution. Therefore, we attribute the values of 0.38 and 0.50 ns (fig. 7.b) as being the intrinsic time resolution of the TFD for the central masses of heavy and light Cf fission fragments. Consequently, such a measurement could be adopted as a quantitative test for timing properties of a TFD.

As to the spectrum of the light output L (Fig. 7.c) obtained with E windows, it gives also characteristic responses for the central masses in heavy and light Cf fission fragments. These responses will be quoted, in the next paragraph, with those obtained from monoenergetic scattered beams.

2.5 RESPONSE OF THE TFD TO MONOENERGETIC HEAVY IONS

The TFD was exposed to beams of ^{16}O , ^{32}S and ^{58}Ni of various energies scattered on an Au target. The TFD was located at an angle of 30° from the beam and at 15 cm from the target. Typical responses of the TFD are shown in figure 8. Fig. 8.a and 8.b display the two cases already explored with Cf source, i.e. the one with a film of an annular shape and the other with a film irradiated at its central part. The comparison of the

two figures confirms the result precedently outlined : an extended film with a hole at its centre gives a wider response but still quite acceptable. Figure 8.c corresponds to a thinner film of $90 \mu\text{g}/\text{cm}^2$. It illustrates the decrease of the response with the thicknesses.

Finally, in figure 9, we present the responses of the TFD to the different ions and to the light and heavy Cf fission fragments selected by E windows. The figure confirms the general trend previously observed by Muga et al. ³⁾ and extend their results to higher energies. It is worth to give the following comments :

- At high energy the responses tend to level off to a constant value for a given ion.
- At low energy the responses to different ions tend to be more closely grouped.
- For a given energy per nucleon, heavier is the ion larger is the corresponding TFD response.

3. COLLECTION OF THE FUSION EVAPORATION RESIDUES WITH SOLENO

At Tandem energies the angular distributions of the fusion evaporation residues are peaked around zero degrees with respect to the beam direction. The angular acceptance of SOLENO ($1^\circ - 10^\circ$) is sufficient to collect a large part of them. In order to control the collected residues the TFD containing an annular film was placed in front of SOLENO at 7.5 cm from the target and the SSD at its focusing plane (Fig. 1). The size of the film which was adopted covered an angular acceptance of $\theta \sim 3^\circ$ to 10° . Smaller values of θ were not taken because they introduce a too high rate of elastic scattering from the target. The obturator and the iris¹⁾ defined the mechanical entrance of SOLENO which was checked to be compatible with the angular acceptance of the film. When the current of SOLENO was set to focus the fusion residues on the SSD, the elastically scattered particles of higher rigidity were focussed behind the SSD and so did not reach it. The electronic system used in this part was the same as the one drawn in figure 3, but the parameter L was not systematically recorded. The control of the light output was performed by changing the threshold of the CFD

following the TFD and by relating its value to the results of figure 9. The two parameters, i.e. the time-of-flight T and the energy E, were recorded in event-by-event mode, for each ion of mass number A producing in the TFD a signal with an amplitude higher than the threshold and focussed with a charge state Q on the SSD. This measurement of T and E allows the calculation of A and Q by the well-known formulae :

$$A = k_1 ET^2 \text{ and } Q = k_2 ET \quad \text{with} \quad k_1 = \frac{2C^2}{u\ell^2} \text{ and } k_2 = \frac{2}{B\rho\ell e} \quad (2)$$

In these expressions, C is the speed of light, ℓ is the flight length, $B\rho$ is the magnetic rigidity of the ion, u is the atomic mass unit and e is the elementary electric charge. When E is expressed in MeV, T in ns, ℓ in m and $B\rho$ in Tm, we obtain : $k_1 = 1.93 \times 10^{-4} \ell^2$ and $k_2 = 2 \times 10^{-3} / (B\rho\ell)$. In fact, in the calculation, $B\rho$ will be replaced by an average value $\langle B\rho \rangle$ corresponding to the current setting of SOLENO. So, the true significance of Q will be $Q B\rho / \langle B\rho \rangle$.

Beams of ^{16}O and ^{32}S were successively used with both ^{12}C and ^{24}Mg targets and fusion evaporation residues of a large range of masses and energies were collected with SOLENO. The identification in mass number A and charge state Q according to the formulae (2) was taken as a tool to study the main properties of SOLENO related to the identification in mass and the transmission.

The experimental conditions corresponding to the collection of residues from the reactions $^{16}\text{O} + ^{12}\text{C}$, $^{16}\text{O} + ^{24}\text{Mg}$, $^{32}\text{S} + ^{12}\text{C}$ and $^{32}\text{S} + ^{24}\text{Mg}$ are summarized in table 2. In figure 10, is given, for $^{16}\text{O} + ^{12}\text{C}$ reaction, an overall view of the experimental results with contour plots in the T-E plane. Apart the upper line which concerns the projectile it is difficult in this plot to recognize the other ions. However, are visible in this plot the ranges covered in time of flight and energy.

In figure 11, are presented for the $^{16}\text{O} + ^{12}\text{C}$ reaction the contour plot in the Q-A plane as deduced by the formulae (2). There is, here, a straightforward global view on the mass and charge state numbers of the ions focussed at once by SOLENO. The width for a given mass number A represents the resolution δA and the width for a given value Q represents the transmitted $B\rho$ band.

3.1 IDENTIFICATION IN MASS AND THE ISOCHRONISM OF SOLENO

The expression of the resolution in mass as derived from the formulae (1) is :

$$\left(\frac{\delta A}{A}\right)^2 = \left(\frac{\delta E}{E}\right)^2 + \left(\frac{2\delta t}{t}\right)^2 + \left(\frac{\delta \ell}{\ell}\right)^2 \quad (3)$$

The term $\delta E/E$ is simply the energy resolution in the SSD. It is expected to be better than 1 % except for heavier ions ($\lambda \geq 30$) of low energy for which response distortions at the end of their paths become relatively important⁽⁵⁻¹⁷⁾. The term $2\delta t/t$ is originating in both of the TFD and the SSD. Considering the values 0.4 - 0.5 ns of δt obtained for Cf fission fragments and the values 100 to 200 ns taken by the time-of-flight when SOLENO is used, we can expect a value of $2\delta t/t$ better than 1 %. The term $\delta \ell/\ell$ describes the isochronism of SOLENO. It originates in the dependence of the flight length ℓ of an ion focussed by SOLENO on its incidence angle at the entrance of SOLENO. The quantity $\delta \ell/\ell$ was expressed⁽¹⁾ in terms of the solid angle $\delta \Omega$ at the entrance of SOLENO by :

$$\frac{\delta \ell}{\ell} = b \delta \Omega \quad \text{with } b = 2.4 \times 10^{-4} / \text{msr} \quad (4)$$

According to this expression, when $\delta \Omega$ varies from 10 to 100 msr, $\delta \ell/\ell$ is expected to vary from 0.24 to 2.4 %.

The experimental identification in A and Q for the four reactions was sufficiently good that we tried to exploit the results for two purposes :

- To extract the contribution of the isochronism of SOLENO to the resolution in mass.
- To search a dependence of the resolution in mass on the energy and the mass number.

Therefore, to study the effect of the isochronism of SOLENO, two measurements for each reaction were carried out corresponding to two different values of $\delta \Omega$, i.e. 20 msr and 70 msr. Obvious effect on the resolution in mass was observed. The full width at height maximum (FWHM) of the peaks in the spectra of mass A were compared. The variation $\delta \ell/\ell$ was deduced and the value of the coefficient b was found to be

$(1.2 \pm 0.1) \times 10^{-4}/\text{msr}$, quite comparable with the predicted value, calculated from the extremities of the range of ℓ .

On the other hand, to study the dependence of the resolution δA on the energy and mass, advantage was taken of the fact that for a given ion of mass A at values of charge state Q correspond to different values of its kinetic energy. Thus, setting windows on the charge state values, in the Q - A plane, A spectra for individual values of Q were obtained. Then, a table of δA with two entries in A and E was prepared. It was striking that there was no important dependence of δA on E (within the ranges of E). So we could represent the content of the table in only one bidimensional plot $(\delta A, A)$ (figure 12). In this figure the results are compatible with a relationship $\delta A/A \approx 1.4\%$ up to $A = 42$, with a tendency of degradation in δA for higher values of A . Finally, taking into account our precedent analysis we believe that when $\delta \Omega \ll 50$ msr the effect of the isochronism becomes small and the resolution δA would be determined equally by the two terms $\delta E/E$ and $2\delta t/t$.

A dependence of the resolution δA on the TFD threshold was investigated. Three values of the threshold corresponding to the readings of 59, 29 and 18 on L scale in figure 9 were tried and gave no significant effect. It is the value corresponding to the reading of 59 which was kept in the rest of the measurements.

3.2 TRANSMISSION OF SOLENO

When the current of SOLENO is set to a given value a certain type of ion emitted from the target can be focussed more or less efficiently on the detector, depending on its B_p value and on its incident angle at the entrance of SOLENO. For our experimental geometry, the dependence of the focussing on B_p and θ is explained in figure 13 by trajectory calculation. In the simple case where ions have an isotropic emission from the target and a uniform distribution in B_p , the counting rate in the detector plotted versus the B_p of the ions gives a bell shape curve called transmission curve. The counting rate is, usually, replaced by the effective solid angle at the entrance of SOLENO. Experimentally, this simple case is realized, equivalently, by placing a monoenergetic α source at the target position and by plotting the counting rate in the detector versus the electric

current. Such an experimental curve was reported in ref. 1 and was interpreted with trajectory calculations.

Here, the relatively broad angular and energetic distribution of the fusion evaporation residues present an acceptable approximation to the simple case. Consequently, given Q and A values, were selected in the Q - A plane (Fig. 11) and the corresponding events were projected onto the Q -axis. In fact, it is the spectrum of $Q B_p / \langle B_p \rangle$ which is obtained. Such a spectrum displays the transmission curve of SOLENO many times associated to the different integer values possible of Q . In figure 14, the transmission curve is displayed twice for $A = 22$ and $Q = 9$ and 10 . In the same figure we reported for comparison the transmission curve calculated with the program GAUSS¹³⁾ for particles emitted isotropically from the target with a uniform distribution in B_p . The experimental and calculated transmission curves are in agreement. This result gives confidence in the quality of heavy ion collection with SOLENO.

3.3 COLLECTION YIELD WITH SOLENO

Two spectra of the mass number A obtained in two different reactions under the conditions of table 2 and with $\Delta\Omega = 20$ msr are shown in figure 15. The predictions of the code ALICE¹⁸⁾ are plotted with dashed lines in the same figure. They reproduce quite well the overall behaviour of the experimental results. In order to evaluate the collection yield with SOLENO the angular and energetic selections of SOLENO were examined.

3.3.1 Angular selection of SOLENO

Using the code LILITA¹⁹⁾, the angular and energetic distributions of the fusion evaporation residues were calculated for the reactions involved in this work. In figure 16 are shown some angular distributions. The fraction of the area of a given distribution falling inside the angular window corresponding to the angular acceptance of SOLENO constitutes the angular efficiency ϵ_a of SOLENO. When we consider the aperture (3.8° - 9.3°) of SOLENO used in the present work, the efficiency ϵ_a takes for the displayed distributions values ranging from 0.47 to 0.64.

3.3.2 Energetic selection of SOLENO

To focus an ion of given Z and A with a large energy distribution centered at a value E_c , the electric current of SOLENO is chosen to focus this ion for an energy equal to E_c and an electric charge equal to the average charge state value corresponding to E_c . In these conditions the expected experimental spectrum consists of several peaks associated to the different populated charge state values. Such peaks with characteristic widths are shown in figure 17, where energy spectra for different selected mass numbers A are displayed. In the same figure, we joined with dotted lines the population percentages of the charge state values versus the energy, which was found sufficiently flat to be approximated by an effective constant value ϵ_{ch} . On the other hand, we presented in the same figure by histograms the predictions of the code Lilita after having corrected them for the energy loss through the target and the film. Precisely, the histograms represent the energy spectra of the residues at the entrance of SOLENO and the experimental spectra represent them at the focussing plane. By comparison, it is seen that the energy selection of SOLENO could be estimated roughly by the ratio ϵ_e of the areas of the experimental to the theoretical curves (after having been reduced to the same height).

Taking into account this analysis in terms of angular and energetic selections, we established table 3 in order to give the collection yield for some residues as being equal to the product of the corresponding efficiencies ϵ_θ , ϵ_{ch} and ϵ_e . According to this analysis the collection of SOLENO for fusion evaporation residues is of the order of 4 to 6 percents. This yield is mostly sensitive to the angular acceptance at the entrance of SOLENO: in particular when the evaporation from the compound nucleus occurs by nucleons and without α -particles, angular acceptance with smaller angles give higher yields especially for residues of larger masses.

4. CONCLUSION

We presented in this paper a TFD-SSD coincident assembly for the identification in mass of the fusion evaporation residues collected by SOLENO. A detailed description of the assembly as well as its test with the fission fragments delivered by a Cf source were given. The linear responses

and the timing performances were examined. In particular, the linear responses of the TFD to the fission fragments and to O, S and Ni beams were compared. When the assembly was associated to SOLENO, it allowed to display the distribution in mass of the fusion evaporation residues in various reactions. The resolution in mass up to $A \approx 50$ was investigated and the effect of the entry aperture of SOLENO on the isochronism was measured. The collection of heavy ions with SOLENO was described and the main factors determining the collection yield were illustrated : the angular selection at the entrance of SOLENO, the characteristics energy selection of SOLENO and the charge state population of the ions.

Improvement of the light collection in the TFD is still possible by installing a second photomultiplier placed symmetrically to the existing one. For cross section measurements the control of the light output of the TFD could be achieved by recording the light response as a parameter, which, in addition, could stand in certain conditions for a ΔE signal.

The use of a TFD-SSD coincident assembly in heavy ion detection was shown in this work to be very practical and powerful. The only known limitations are due to the damage of the SSD by high rate counting. In such conditions the SSD should be replaced by a gaseous detector.

The authors would like to acknowledge J.C. ARTIGES for his constant help and for preparing the voltage preamplifier ; they thank A. RICHARD and L. STAB for valuable discussions and the tandem crew for the efficient running of the accelerators.

REFERENCES

- 1) J.P. SCHAPIRA, S. GALES and H. LAURENT, Orsay, internal report IPNO-PhN 7921.
J.P. SCHAPIRA, F. AZAIEZ, S. FORTIER, S. GALES, E. HOURANI,
J. KUMPULAINEN and J.M. MAISON Nucl. Instr. and Meth. 224(1984)337.
- 2) M.L. MUGA, Nucl. Instr. and Meth. 95(1971)349.
- 3) L. MUGA and G. GRIFITH, Phys. Rev. B9(1974)3639.
- 4) R.K. BATRA and A.C. SHOTTER, Nucl. Instr. and Meth. 124(1975)101.
- 5) T. BATSCH and M. MOSZYNSKI, Nucl. Instr. and Meth. 123(1975)341.
- 6) S.C. GUJRATHI and L. LESSARD, Nucl. Instr. and Meth. 206(1983)183.
- 7) R.K. BATRA and A.C. SHOTTER, Nucl. Instr. and Meth. B5(1984)14.
- 8) C. MANDUCHI, M.T. RUSSO-MANDUCHI and G.F. SEGATO, Nucl. Instr. and Meth. A243(1986)453.
- 9) C.K. GELBKE, K.D. HILDENBRAND and R. BOCK, Nucl. Instr. and Meth. 95(1971)397.
- 10) J.M. NICOVICH, A. CLEM, L. MUGA and H.S. PLENDL, Nucl. Instr. and Meth. 157(1978)93.
- 11) E. HOURANI, J. KUMPULAINEN, F. AZAIEZ, S. FORTIER, S. GALES,
J.M. MAISON and J.P. SCHAPIRA, Proc. of the XXII Int. Meeting on Nucl.
Phys. p. 432, 1984, Bormio, Italy.
- 12) J. KUMPULAINEN, Thesis, 1985, University of Jyväskylä, Finland.
- 13) H.W. SCHMITT, W.E. KIKER and C.W. WILLIAMS, Phys. rev. 137(1965)B837.
- 14) H.W. SCHMITT and F. PLEASANTON, Nucl. Instr. and Meth. 40(1966)204.
- 15) T.H. ZABEL, M.P. FEWELL, D.C. KEAN, R.H. SPEAR and A.M. BAXTER, Nucl.
Instr. and Meth. 174(1980)459.
- 16) T. KITAHARA, H. GEISSEL, Y. LAICHTER and P. ARMBRUSTER, Nucl. Instr.
and Meth. 196(1982)153.
- 17) E. KLEMA, F.J. CAMELIO and T.K. SAYLOR, Nucl. Instr. and Meth.
225(1984)72.
- 18) M. BLANN, Overlaid Alice, Univ. Rochester, Report n° C00-3493-29,
1976.
- 19) J. GOMEZ DEL CAMPO and R.G. STOKSTAD, Description and use of the Monte
Carlo code LILITA, unpublished ;
J. GOMEZ DEL CAMPO, R.G. STOKSTAD, J.A. BIGGERSTAFF, R.A. DAYRAS, A.H.
SNELL and P.H. STELSON, Phys. Rev. C19(1979)2170.

Parameters	This work (slowed FF)	Expected values ^{1,4)} (unslowed FF)	From ref.7 (slowed FF)
N_L/N_V	2.78	~ 2.90	2.26
N_H/N_V	2.32	~ 2.20	2.13
N_L/N_H	1.20	~ 1.30	1.15
$\Delta L/(L-H)$	0.39	~ 0.36	0.44
$\Delta H/(L-H)$	0.43	≤ 0.44	0.51
$(H-H_S)/(L-H)$	0.65	≤ 0.69	0.69
$(L_S-L)/(L-H)$	0.50	≤ 0.48	0.57
$(L_S-H_S)/(L-H)$	2.16	~ 2.17	2.26

Table 1 : Values of the parameters of Schmitt and Pleasonton describing the SSD response to ²⁵²Cf fission fragments.

Position of the target from the median plane of the iron shield of SOLENO	-1.005 m
Position of the Si detector from the same plane	1.375
Opening of the detector	φ 17 mm
Incident beams	^{16}O (87.5 MeV) ^{32}S (121 MeV)
Targets	C (50 $\mu\text{g}/\text{cm}^2$) ^{24}Mg (100 $\mu\text{g}/\text{cm}^2$)
Angular acceptance of SOLENO	$\theta = 5.3^\circ - 7^\circ \Delta\Omega = 20 \text{ msr}$ $\theta = 3.8^\circ - 9.3^\circ \Delta\Omega = 70 \text{ msr}$
Current settings of SOLENO	$B\rho = 0.481 \text{ T}\cdot\text{m} \quad (\text{O} + \text{C})$ $B\rho = 0.396 \text{ T}\cdot\text{m} \quad (\text{O} + \text{Mg})$ $B\rho = 0.506 \text{ T}\cdot\text{m} \quad (\text{S} + \text{C})$ $B\rho = 0.469 \text{ T}\cdot\text{m} \quad (\text{S} + \text{Mg})$

Table 2 : Experimental conditions used in the study of the collection with soleno of the fusion-evaporation residues produced in the reactions O+C, O+Mg, S+C and S+Mg.

Reaction	Energy (MeV)	Mass number of the residue	Angular efficiency ϵ_{θ}	Charge state efficiency ϵ_{cb}	Energetic efficiency ϵ_E	Collection yield
$^{16}\text{O} + ^{24}\text{Mg}$	87.5	36	0.64	0.24	0.40	0.061
$^{32}\text{S} + ^{12}\text{C}$	121	38	0.60	0.22	0.40	0.052
$^{32}\text{S} + ^{24}\text{Mg}$	121	50	0.47	0.20	0.40	0.038

Table 3 : Estimation of the collection yield of SOLENO for some fusion evaporation residues. The collection yield was calculated as the product of three independent factors ϵ_{θ} , ϵ_{cb} and ϵ_E (see text).

FIGURE CAPTIONS

- Fig. 1 : Experimental set up with the superconducting solenoidal coil SOLENO used as a recoil mass spectrometer. Numbers label different parts of SOLENO : 1 - iron shield ; 2 - coil ; 3 - Faraday cup ; 4 - baffle ; 5 - vacuum chamber.
- Fig. 2 : Drawing of the mounting of the film on its frame and of its position relatively to the target (or the source) : 1 - film ; 2 - Al plate ; 3 - Cu wire ring ; 4 - light reflector.
- Fig. 3 : Diagram of the electronic set up. The abbreviations denote the following devices : TFD-thin film scintillator detector, SSD-solid state Si detector, PM-photomultiplier, FO-Fan out, CFD-constant fraction discriminator, LGS-linear gate and stretcher, VPA-voltage preamplifier, CPA-charge preamplifier, LA-linear amplifier, TAC-time to amplitude converter, L-light output, T-time-of-flight and E-energy.
- Fig. 4 : Light responses of the $160 \mu\text{g}/\text{cm}^2$ TFD to ^{241}Am and ^{252}Cf sources : a) response to the α -particles from Am, b) response to the α -particles and fission fragments from Cf and c) as in (b) but with annular film.
- Fig. 5 : Energy spectrum of the slowed ^{252}Cf fission fragments measured with the SSD. Some characteristic quantities are defined.
- Fig. 6 : Two-dimensional contour plots of the three correlated parameters, L, E and T with the Cf fission fragments. (c) is obtained for windows set in E as shown in figure 7. Contour levels were taken at the number of counts indicated.

- Fig. 7 : Projected spectra of the correlated E, T and L obtained with Cf fission fragments. In (a) all the correlated events were taken. In (b) and (c), upper curves correspond to all the correlated events whereas lower curves correspond to events falling inside the windows defined in (a).
- Fig. 8 : Response of films to ^{58}Ni of 50 MeV : a) annular film of $160 \mu\text{g}/\text{cm}^2$ b) normal film of $160 \mu\text{g}/\text{cm}^2$ irradiated at its central part and c) normal film of $90 \mu\text{g}/\text{cm}^2$.
- Fig. 9 : Responses of the TFD (at the central part) of $160 \mu\text{g}/\text{cm}^2$ vs the energy, measured with O, S and Ni beams and with light and heavy ^{252}Cf fission fragments. The total error bar in each point represents the FWHM of the corresponding TFD response.
- Fig. 10 : Contour plots in the T-E plane for the $^{16}\text{O} + ^{12}\text{C}$ reaction. The upper line is constituted by the scattered projectiles, the rest being the fusion evaporation residues. Contour levels at 10, 100 and 220 counts.
- Fig. 11 : Contour plots in the Q-A plane for the reaction $^{16}\text{O} + ^{12}\text{C}$. The experimental conditions are summarized in table 2. The well-isolated vertical line on the left was identified as being due to the projectile and was then used to identify in A and Q the rest. Contour levels are at 10, 50, 150 and 250 counts.
- Fig. 12 : The resolution in mass δA versus A. The points represent the FWHM of peaks observed experimentally in the A spectra for the different reactions. The dashed line serves to guide the eye.

- Fig. 13 : Two-dimensional plot of the magnetic rigidity $B\rho$ (normalized to the central value $\langle B\rho \rangle$) of the incident ions and of their incident angle θ with respect to the axis of SOLENO. Hatched area define the $B\rho$ and θ values for which ions are focussed on the detector : the corresponding calculated trajectories (i) get through the entrance of SOLENO (between the iris and the obturator), (ii) do not intersect the walls of the vacuum chamber and (iii) have transversal elongations at the detector position lying between $-R_D$ and R_D , R_D being the radius of the detector.
- Fig. 14 : The $Q \cdot B\rho / \langle B\rho \rangle$ spectrum for the residue of $A=22$ and $Q=9$ and 10 obtained in the $^{16}O + ^{12}C$ reaction at 87.5 MeV. In rounds are plotted the results of the code GAUSS for the calculation of the transmission curve. The calculation was made accordingly to the experimental conditions for θ ranging from $3,8^\circ$ to $9,3^\circ$ and it gave at the maximum the expected value of 70 msr.
- Fig. 15 : Spectra of the mass number A for two reactions : (a) the reaction $^{16}O + ^{12}C$ and (b) the reaction $^{32}S + ^{24}Mg$. The experimental conditions are given in table 2. Here $\Delta\Omega$ was 20 msr. In dashed lines are the results of the code ALICE.
- Fig. 16 : Angular distributions of some residues at the incident energies given in table 2, calculated by the code LILITA.
- Fig. 17 : Energy spectra for some residues obtained under the conditions of table 2 in the following reactions : (a) $^{16}O + ^{24}Mg$ with $\Delta\Omega = 70$ msr (b) $^{32}S + ^{12}C$ with $\Delta\Omega = 20$ msr and (c) $^{32}S + ^{24}Mg$ with $\Delta\Omega = 20$ msr. In dotted lines are the charge state population in arbitrary units. In dashed lines are the results of the code LILITA reduced to the height of the corresponding experimental results.

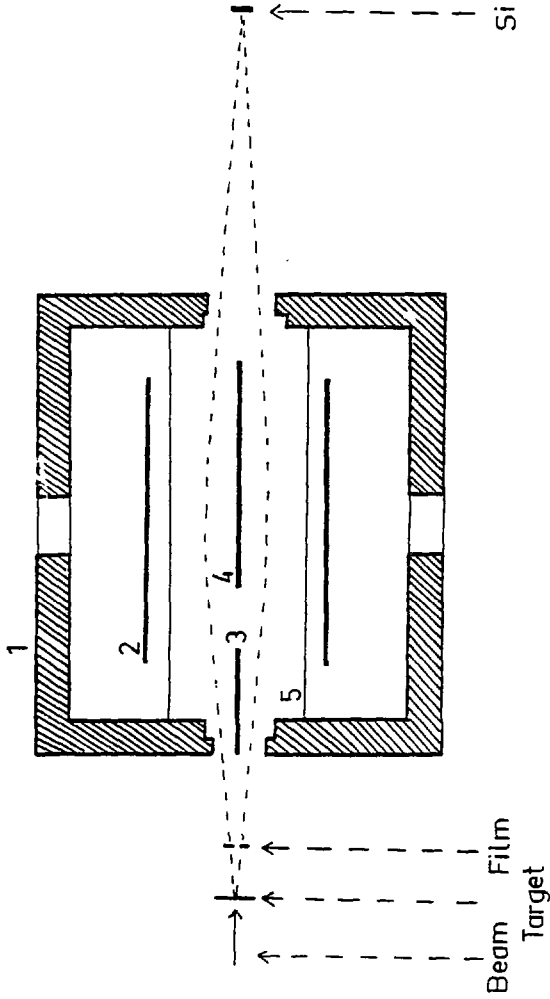
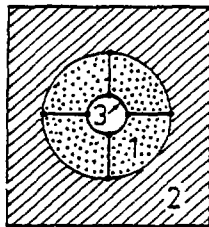
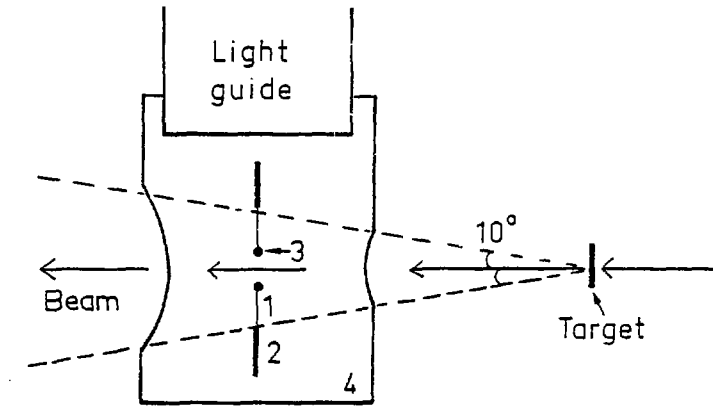


Fig. 1



Film frame

Fig. 2

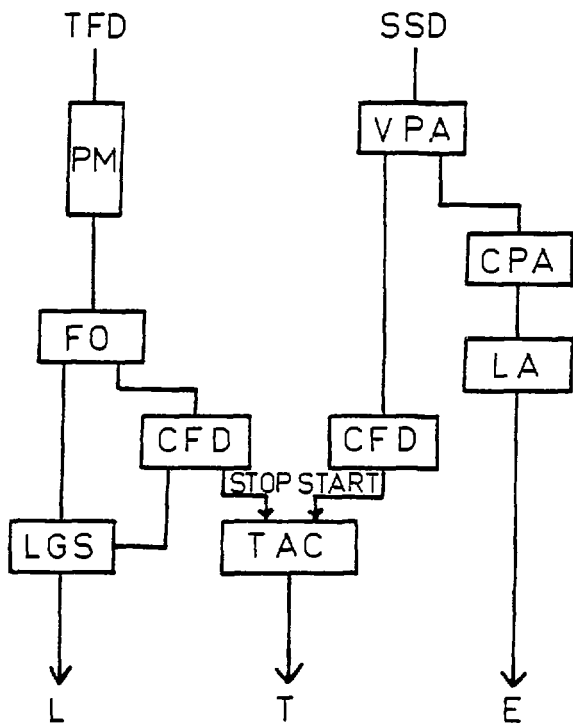


Fig. 3

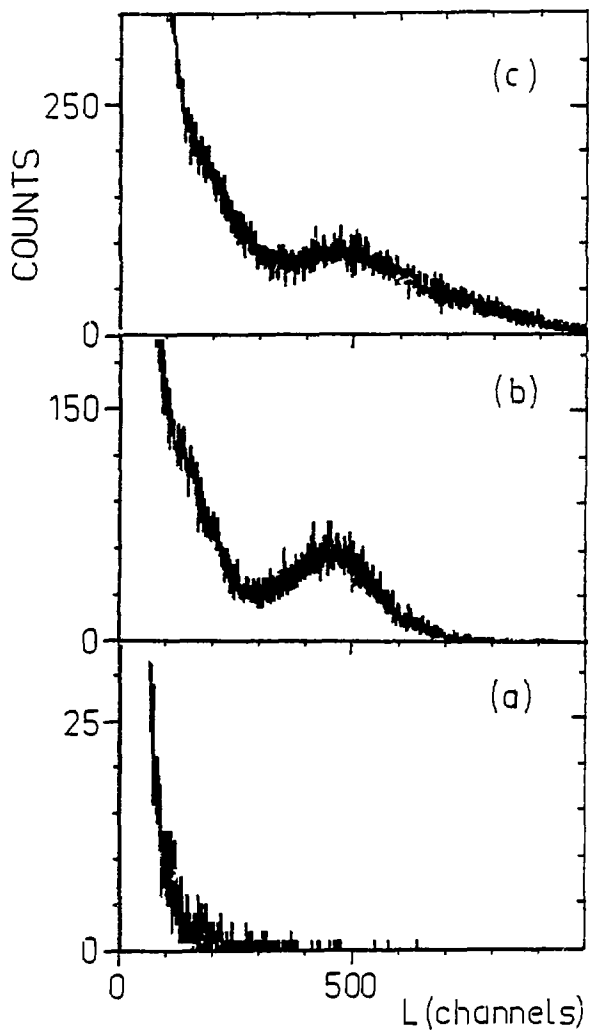


Fig. 4

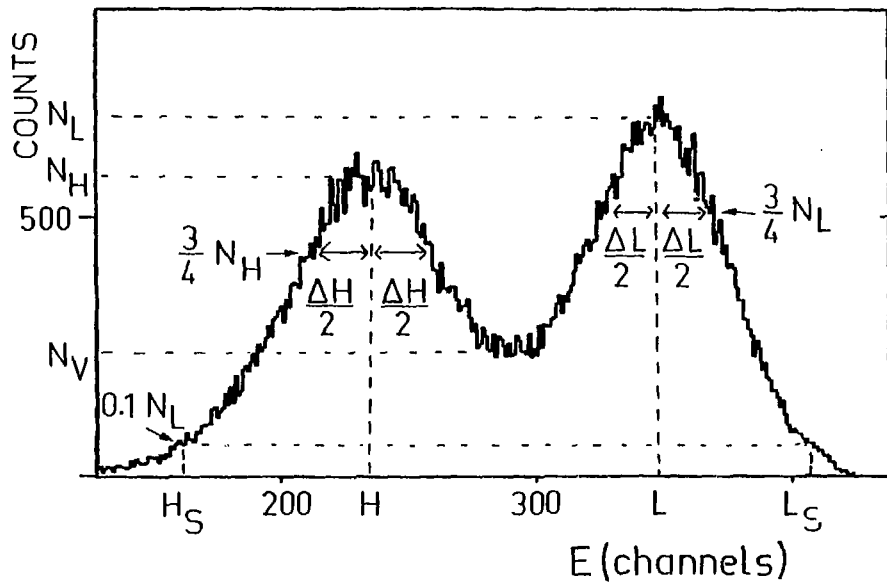


Fig. 5

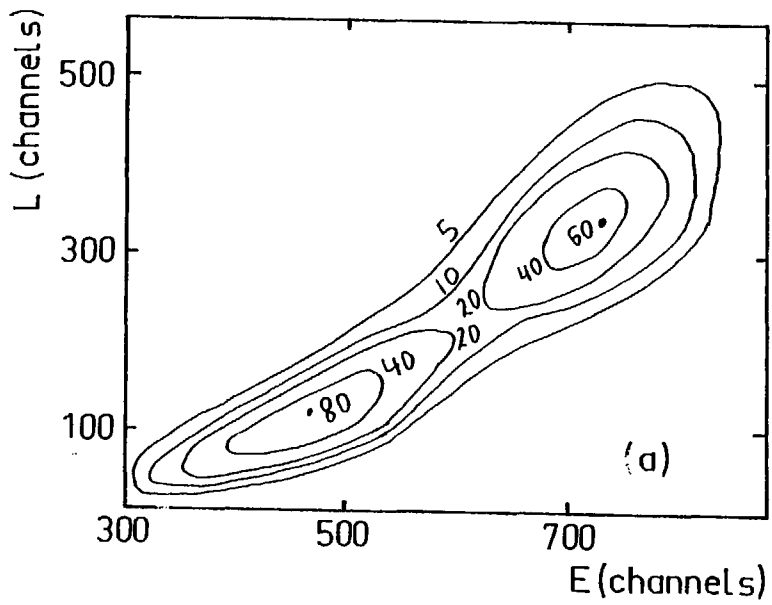


Fig. 6-a

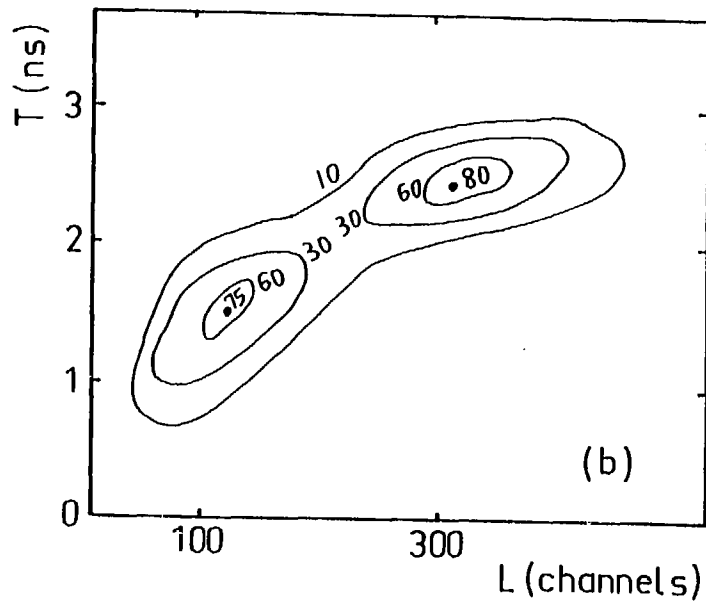


Fig. 6-b

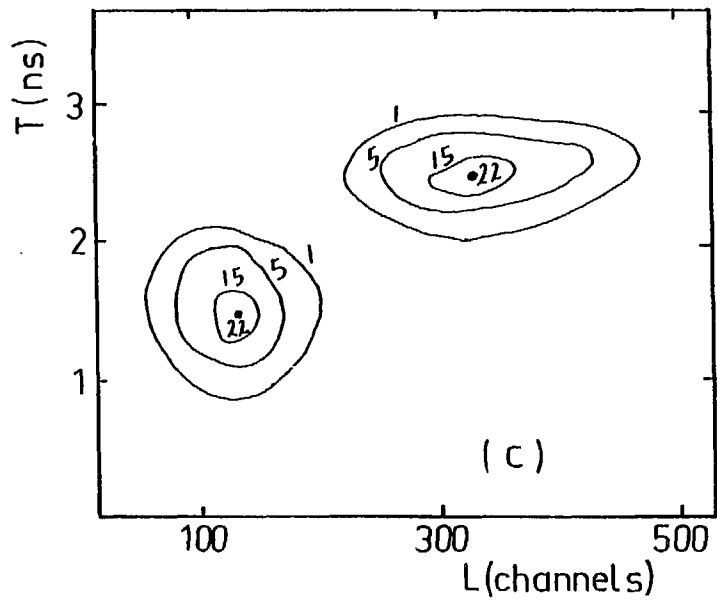


Fig. 6-c

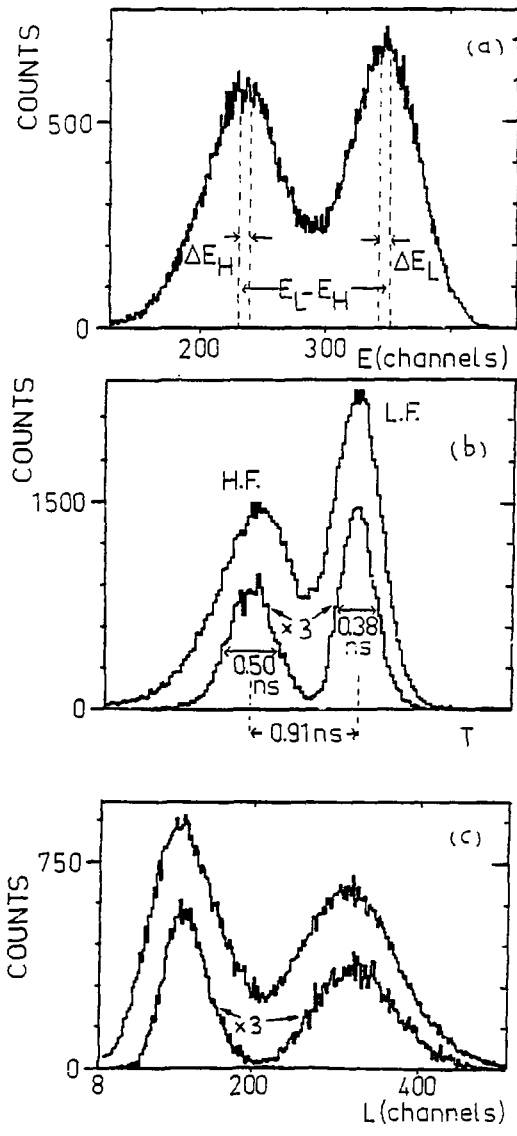


Fig. 7

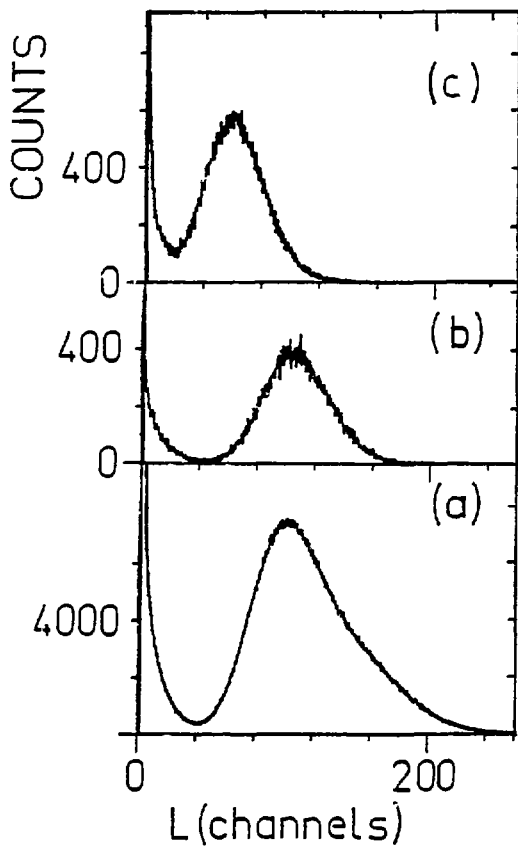


Fig. 8

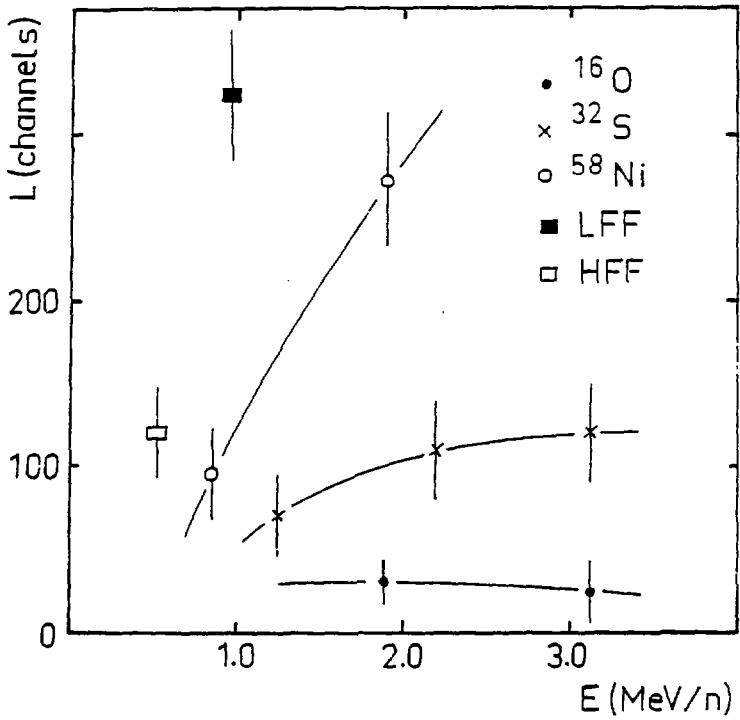


Fig. 9

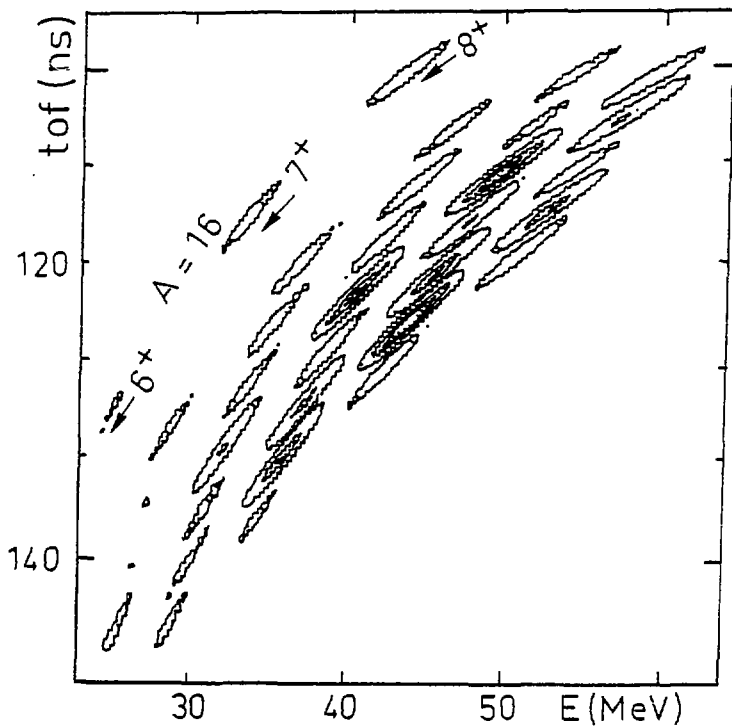


Fig. 10

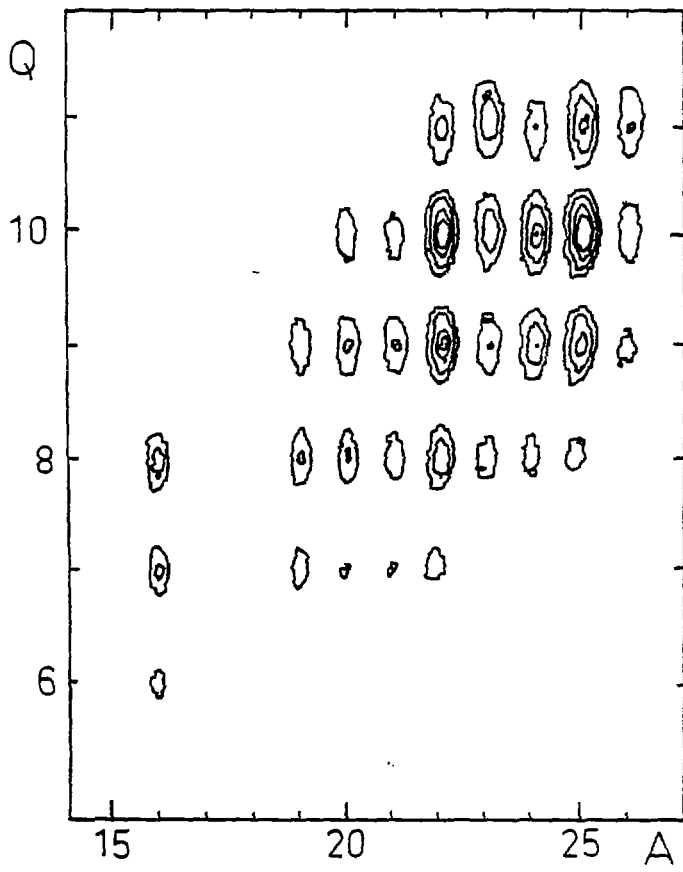


Fig. 11

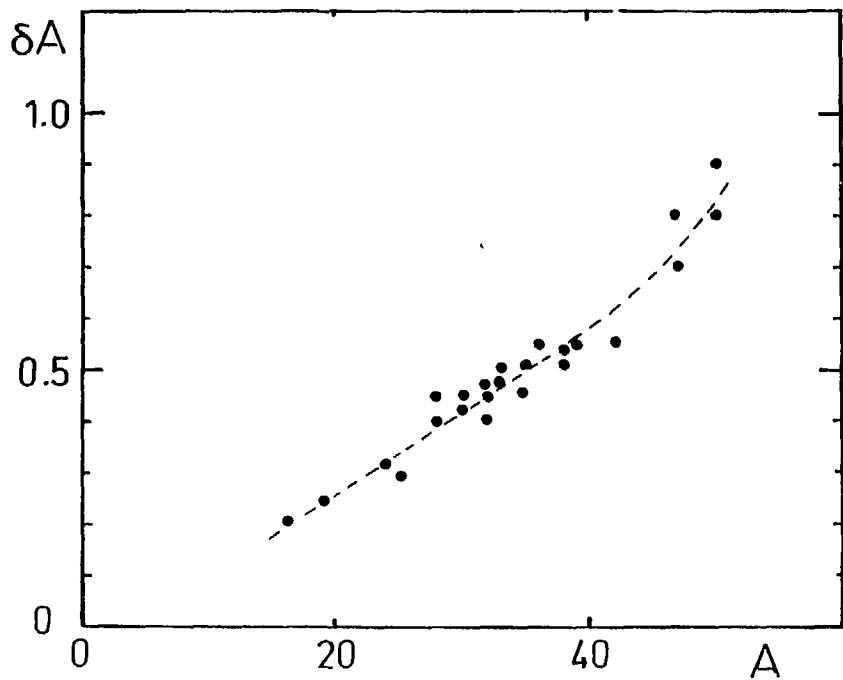


Fig. 12

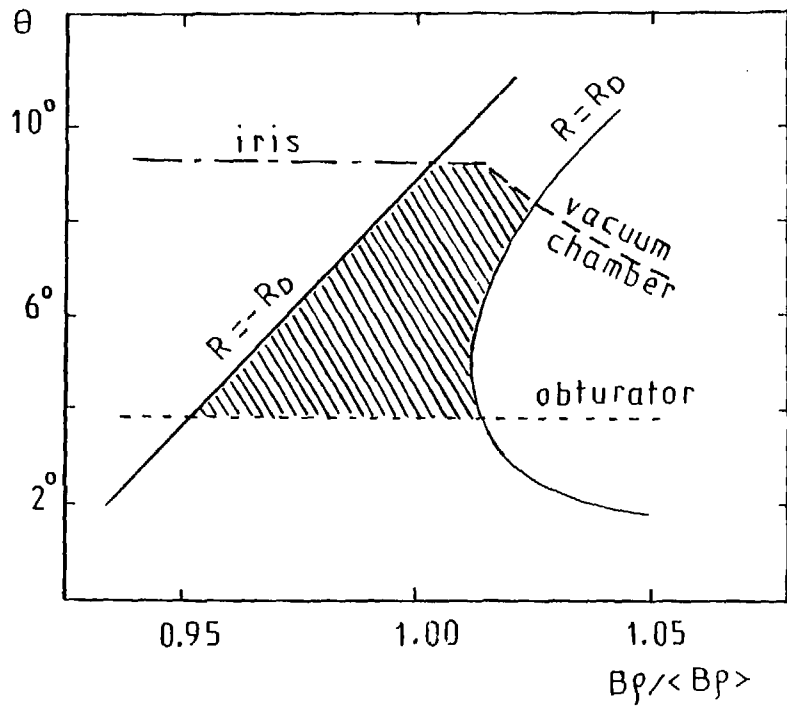


Fig. 13

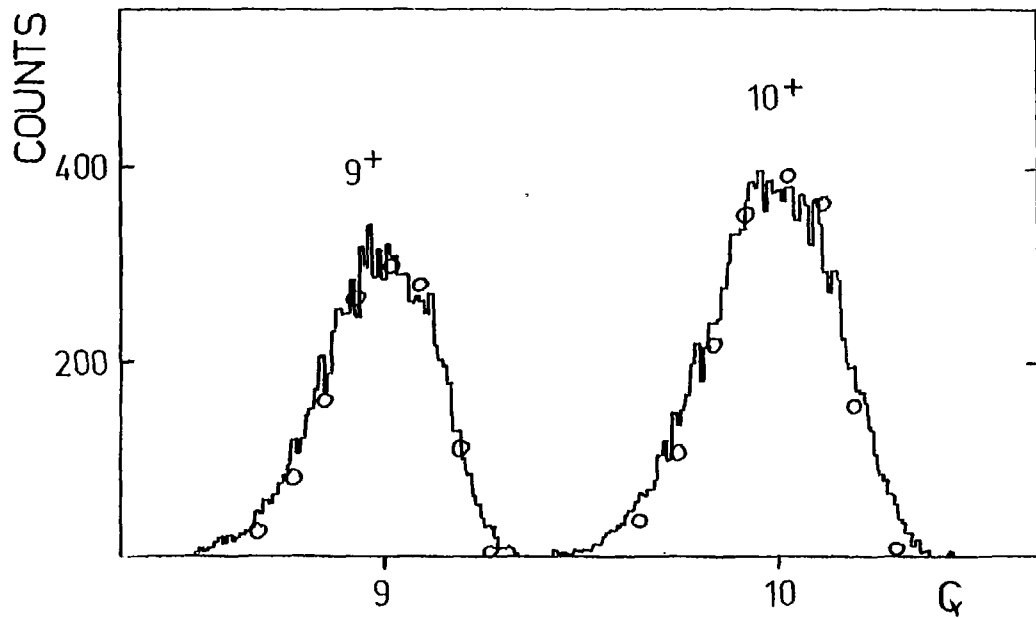


Fig. 14

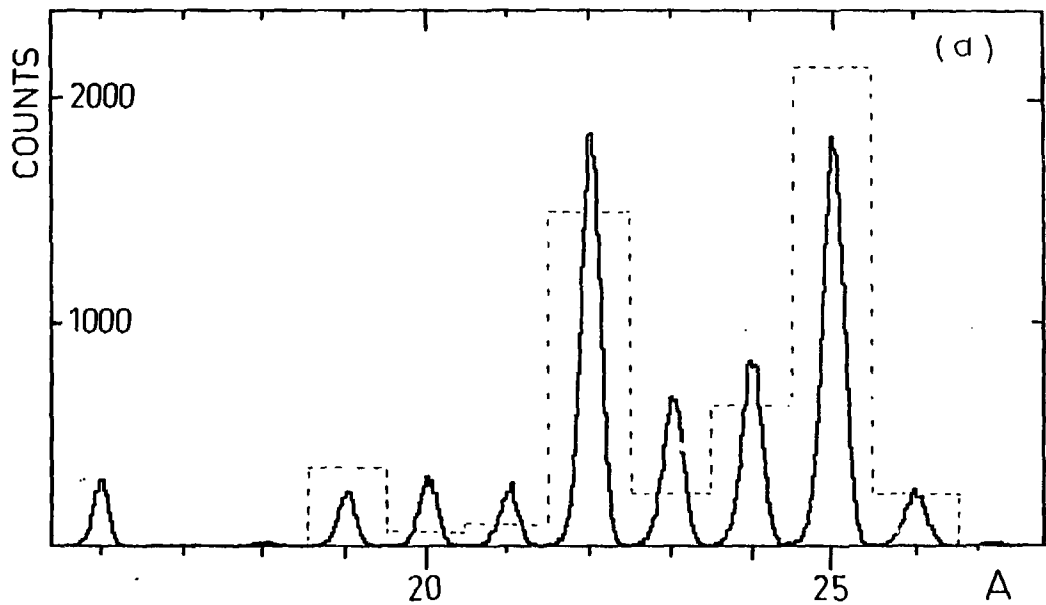


Fig. 15-a

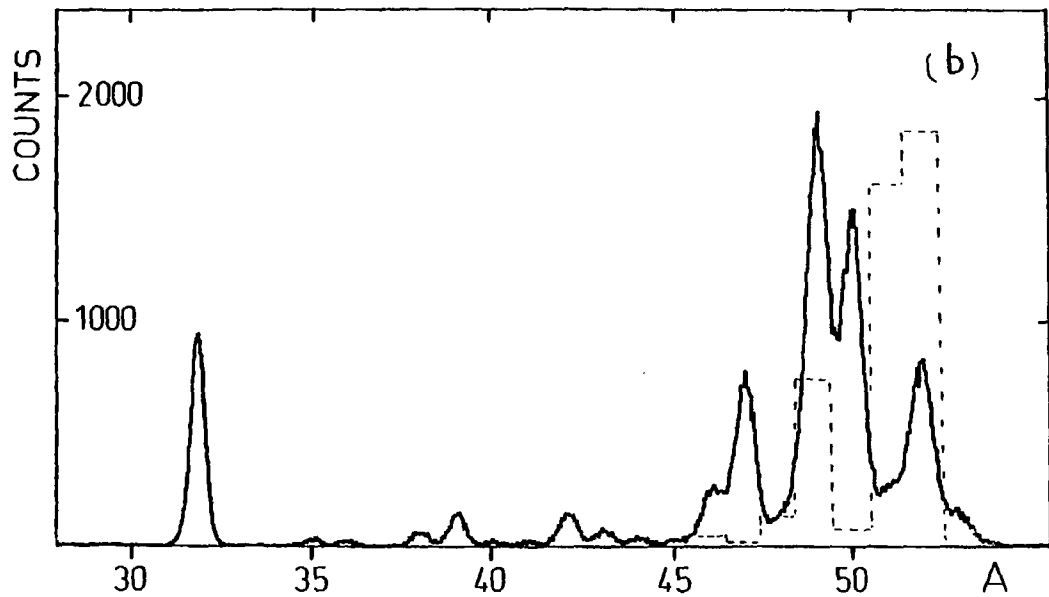


Fig. 15 - b

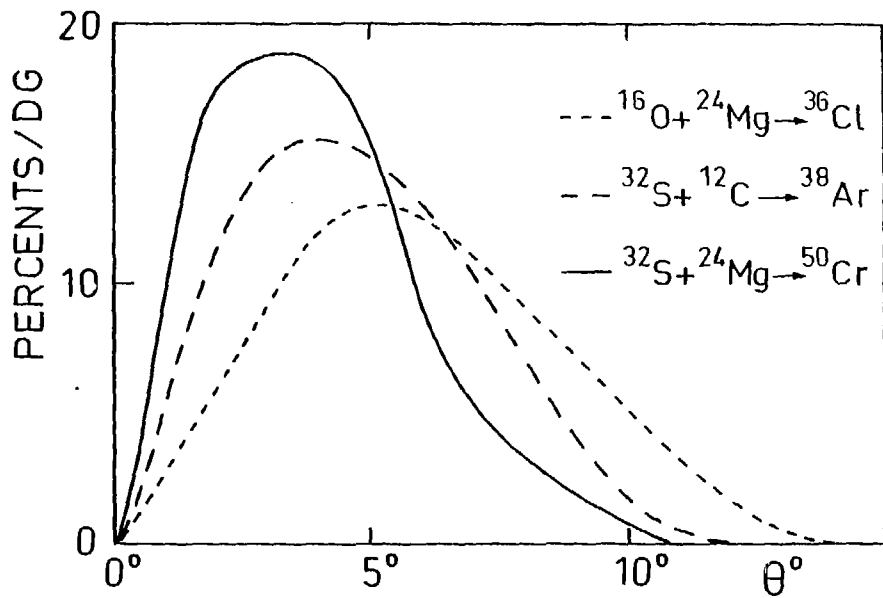


Fig. 16

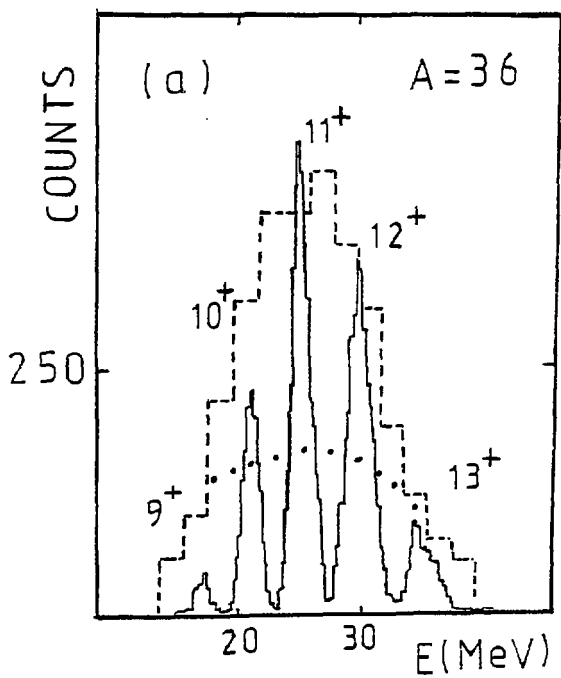


Fig. 17-a

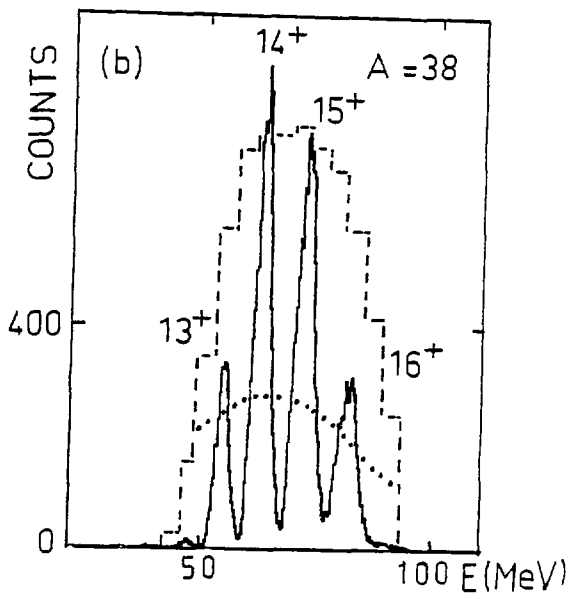


Fig. 17 - b

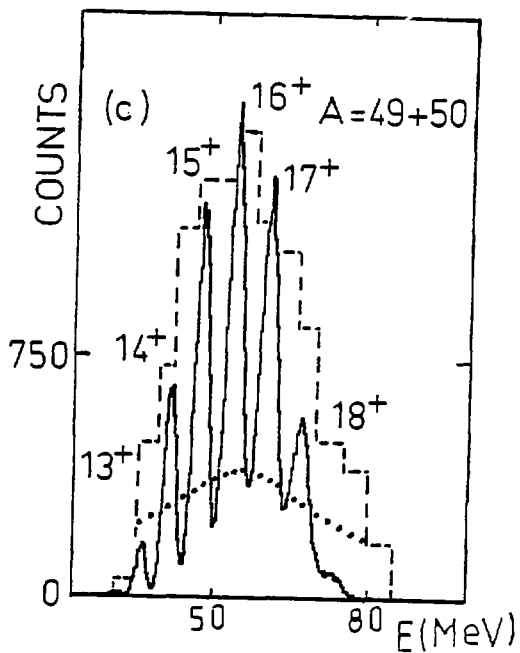


Fig. 17-C